Journal of Electrical Engineering & Technology (2023) 18:1733–1743
https://doi.org/10.1007/s42835-022-01322-w

ORIGINAL ARTICLE

Cogging Torque Minimization of PMBLDC Motor for Application in Battery Electric Vehicle

Rupam Bansal[1] · **Sanjay Marwaha**[1] · **Chaman Verma**[2]

Received: 13 May 2022 / Revised: 19 October 2022 / Accepted: 10 November 2022 / Published online: 30 November 2022

Abstract
Since the beginning, researchers have focused globally on the automotive industry, which recently yielded a notable increase in the development of electric vehicles. The cogging torque of the motor is the leading cause of acoustic noise and vibration. Therefore, this paper aims to reduce the cogging torque of Brushless DC motors in electric vehicles. The power rating of the two-wheeler battery electric vehicle is determined with kinematic dynamic equations. The choice of material and the combination of pole slots impact the vehicle's overall performance, particularly in raising the average torque of the motor. Finite element based Ansys Maxwell electromagnetic field simulation software has been used to design and analyze the electric and magnetic field parameters of BLDC motor using several rotor poles embrace factor values. The findings of this study are expected to reduce vibration and noise in electric vehicles with increased average torque.

Keywords Permanent magnet motor · BH curve · Silicone steel · Battery electric vehicle

1 Introduction

In recent years, poor air quality has diverted the scientific community's interests toward Electric Vehicles (EVs), which can potentially reduce fuel costs and overpower the current energy crisis. Electric motors play a crucial role among the various components of the Battery Electric Vehicles (BEV's) architecture. Electric motors are expected to provide maintenance-free operation, high power density, wide-speed range, and high efficiency [1, 2]. Because of excellent reliability and low-cost traditional motors, the induction machine is still extensively acknowledged [3]. However, conventional control approaches in EVs cannot deliver the requisite performance. Conventional motors can also perform well with the current drive designs, but they are less viable with their inefficiencies in the lower speed ranges. The reason behind it is high losses and limited constant power range [4]. Nowadays, Permanent magnet motors are more competitive, especially permanent magnet brushless direct current (PMBLDC) motors that have a wide range of applications [5]. Fortunately, there have been many positive reviews on PMBLDC motors available in the literature, especially in the category of commutator-less machines. This motor has many features like simple structure, good mechanical characteristics, high efficiency, lightweight, low rotary inertia, high control precision and operates at low speed. However, demagnetization and cogging torque are some of the limitations of this motor [6–9].

Selection of materials, dimensions and design variations are essential parameters usually considered for motors. The first step for executing good design is to thoroughly understand the design process and make amendments as per the required applications. With the increasing use of high-power computing systems, the development of computational electromagnetics is also energized. Before performing things in the real world, these electromagnetic investigations of problems through computation will save time and money [10]. Numerical methods are used to solve the behavioural equations of electrical machines. The finite element method

✉ Chaman Verma
chaman@inf.elte.hu

Rupam Bansal
rupamb92@gmail.com

Sanjay Marwaha
marwaha_sanjay@yahoo.co.in

[1] Department of Electrical and Instrumentation Engineering, Sant Longowal Institute of Engineering and Technology, Sangrur, Punjab, India

[2] Department of Media and Educational Informatics, Faculty of Informatics, Eötvös Loránd University, Budapest 1053, Hungary

(FEM) numerical technique is one of the most reliable, flexible, and worthwhile for analyzing performance of electrical machines. Electromagnetic analysis of machines allows the determination of flux leakage distributions in a steady state at the areas of concern. As regards the magnetic vector potential, the magnetic field of electrical machines is analyzed using FEM, which allows for simple flux and flux density determination [11–14]. The reason is that complex geometries can easily be modelled and analyzed, which is impossible with other numerical techniques. Without significant knowledge of applied mathematics, this technique can be used to determine electromagnetic field distribution and critical parameters in the design of the rotating machine. Extensive research has been done on the design of motors using FEM [15–17].

From recent literature- The permanent magnet motor surface-mounted was designed by selecting an appropriate combination of pole arc coefficient, rotor pole, and stator slot with the help of FEM. Losses of the motor were determined based on electromagnetic torque [18]. The author mentioned a light electric vehicle drive system. The flux switching outer rotor type permanent magnet machine of 6 slots in the stator and 19 poles on the rotor with 188 W and 120 rpm combination was built for the application using a sizing equation and based on a finite element approach. The calculation of magnetic field distribution and machine parameters was done, and then performance was analyzed by the current vector strategy [19]. The authors illustrated motor design for application of three-wheeler. The results are obtained using a computer-aided finite element analysis tool to get the electromagnetic features of the motor [4]. In another study, the author proposed the design of BLDC, where pole arc coefficient and air gap length were optimized for medium-speed electric vehicles. Two-dimensional models were analyzed using Ansys Maxwell [20]. The author proposed the design of the motor and generator based on the three design variables. The thermal analysis was conducted, and fabrication of the structure was completed [21]. The author proposed some changes in the prior winding, which enhanced the performance of the motor depending on the material used and losses occurring in set up reduced considerably [22]. The Axial Flux type BLDC motor on Surface mounted type (AFSPMBLDC) motor was designed using a genetic algorithm. The aim of this analysis was to give the best possible combination of design variables acquired by employing the optimization technique genetic algorithm (GA), and the motor design depends on these optimized design factors. The validation at the end was carried out with 3D type finite element analysis (FEA) [23]. The author proposed the design for the motor for the micro-electric vehicle with the help of electromagnetic analysis [2]. The author proposed a BLDC motor design for light electric vehicles. This summarized that the proposed design type has the best result for the required application [24]. In another study, the author proposed a new method which includes superposition and subdomain methods to determine the cogging torque with rotor eccentricity of the permanent magnet motor. Using Maxwell stress tensor, cogging torque and effectiveness had been illustrated with FEA on 9slot/8pole and 12slot/10pole motor [25]. In this paper, author has emphasized only on wind power permanent synchronous generators with static and rotating eccentricity. In another paper [26], the authors proposed the design of a BLDC motor by applying the Artificial Neural Network and FEM method. The ratio of pole arc to pole pitch and values of offset were altered to achieve the required result of the motor. The authors in this paper have mainly concentrated their efforts on fast optimization of solutions based on Particle Swarm Optimization and Imperialist Competitive Algorithm. Still, they have not discussed the practical implications caused by dynamic conditions.

The present work deals with the parameter estimation of the PMBLDC motor with emphasis on reducing cogging torque and improving average torque of motor used in two-wheelers battery electric vehicles. The matching material and pole-slot combination are selected for the motor, which yields low cogging torque. PMBLDC model has been simulated considering the distinct values of the pole embrace factor design variable using a computational electromagnetic tool, i.e., Ansys Maxwell. Further, the paper's focus is to carry out the improvements in design by performing parametric analysis. The final model offers a reduction in torque ripple with improved average torque. Because of the finite element adaptive approach, the design variable gets updated if changes are observed in computed and reference parameters of the motor. In the later part of the manuscript, simulation results and comparisons between the base design [24] and the proposed motor design have been discussed.

2 Parameter Matching of BEV

The dynamic equations are taken to match the performance of the BEV with the PMBLDC motor. The EV characteristics can be used to calculate the vehicle's driving resistive forces along with the help of initial assumed parameters. Based on dynamic vehicle equations, the torque and power requirements have been derived for the specific driving condition [27, 28]. The forces acting on the vehicle are shown in the schematic presentation Fig. 1.

2.1 Kinematic Dynamic Equations

Equations regarding different kinds of forces acting on the vehicle and tractive power and torque have been briefly discussed.

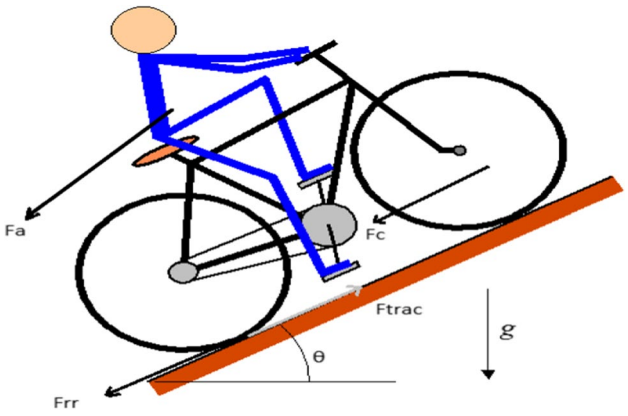

Fig. 1 Representation of forces acting on a vehicle

2.1.1 Aerodynamic Drag Force

The aerodynamic drag force (F_a) in (1) is because of the friction of the vehicle moving through the air. The drag coefficient is C_d, the vehicle's velocity is v, and rho (δ) is the air density at sea level. This force is directly square to a vehicle's velocity, frontal area, and body shape.

$$F_a = \frac{1}{2}\delta \quad A \quad C_d v^2 \tag{1}$$

2.1.2 Rolling Resistance Force

The rolling resistance force (F_{rr}) in (2) depends on the tire's selection. The rolling resistance coefficient is u_{rr}, the gravitational force is g, and the gradient angle is Θ. This force is directly proportional to the coefficient of rolling coefficient.

$$F_{rr} = mg\ \mu_{rr}\ Cos\theta \tag{2}$$

2.1.3 Climbing Force

The climbing force (F_c) in (3) is needed to propel the vehicle up a slope where the vehicle's gross weight is m.

$$F_c = mg\ Sin\theta \tag{3}$$

2.1.4 Total Tractive Force

The total tractive force (F_{trac}) in (4) combines all the resistive forces needed to overcome the friction.

$$F_{trac} = F_a + F_{rr} + F_c \tag{4}$$

2.1.5 Tractive Power

The tractive power in (5) can be calculated and represented as (P_{trac})

$$P_{trac} = F_{trac} v \tag{5}$$

2.1.6 Tractive Torque

The force in (6) calculates the tractive torque (T_{trac}) on the vehicle wheel. Here r_{wheel} is the radius of the vehicle wheel.

$$T_{trac} = F_{trac} * r_{wheel} \tag{6}$$

The reference vehicle taken is a two-wheeler having values of the parameters like gross weight, air drag coefficient and rolling coefficient, etc., as shown in Table 1.

The Indian driving cycle (IDC) selected for this vehicle is shown in Fig. 2.

3 Mathematical Modelling of PMBLDC Motor

The sizing for electrical machine design is given by (7).

$$S = 11.k_{w1}.B.ac.\left(\frac{D}{100}^2\right).\frac{L}{1000}.n \tag{7}$$

where S is motor apparent power in VA, k_{w1} is winding factor, B is magnetic specific loading, electrical specific loading is ac, L is stack length, D is stator diameter, n is rated speed of the motor. The modelling of the PMBLDC motor is proposed keeping in view that undesirable cogging torque that leads to inefficient operation. In the PMBLDC motor, the cogging torque affects average torque and generates unwanted torque ripple. The cogging torque as stated in (8) must be lowered to reduce noise and vibration [29, 30].

Table 1 Specifications of Initially selected parameters for BEV

Parameter	Value
Gross weight (m)	250 Kg
Specific acceleration (g)	9.81 m/s^2
Coefficient rolling resistance (μ_{rr})	0.004
Radius of the vehicle wheel (r_{wheel})	0.216 m
Density of air (δ)	1.23 Kg/m^3
Drag coefficient (Cd)	0.88
Driving Cycle	IDC
Velocity (v)	50 Km/h
Gradient (Θ)	0 Deg

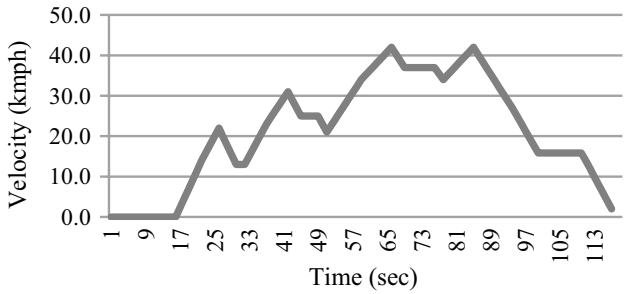

Fig. 2 Graphical representation of two-wheeler-IDC

$$T_{cog} = \frac{1}{2}\theta_g^2 \frac{dR}{d\theta} \tag{8}$$

where air gap flux is θ_g and change in air gap reluctance (as a rotor angle depends) is $\frac{dR}{d\theta}$. The cogging torque will be reduced by reducing $\frac{dR}{d\theta}$ as they are directly proportional to each other. The calculation of the cogging torque is based on changing one mechanical degree of angular rotation. It's worth noting that most cogging torque-reduction solutions also diminish the effective back electro-motive force (emf), resulting in the generation of mutual torque. The voltage equation of three-phase a, b and c of PMBLDC motor equivalent circuit in matrix form is shown in (9).

$$\begin{cases} V_a = i_a R + L\frac{di_a(t)}{dt} + e_a \\ V_b = i_b R + L\frac{di_b(t)}{dt} + e_b \\ V_c = i_c R + L\frac{di_c(t)}{dt} + e_c \end{cases} \tag{9}$$

In compact form the equation can be expressed in (10) where $\widehat{V}$ is the phase voltage, $\widehat{I}$ is phase current and $\Delta\widehat{I}$ is the change in phase current with respect to time.

$$\widehat{V} = f\left[\widehat{I}, \Delta\widehat{I}\right] \tag{10}$$

The back-EMF values are affected by the number of rotations, rotor speed, and magnetic field intensity. There is a phase difference of 120° between each phase of the three-phase system. If the back-EMF constant is λ, then the back-EMF for each phase's value is described as in (11).

$$\begin{aligned} e_a &= \omega\lambda(\theta) \\ e_b &= \omega\lambda\left(\theta - \frac{2\pi}{3}\right) \\ e_c &= \omega\lambda\left(\theta + \frac{2\pi}{3}\right) \end{aligned} \tag{11}$$

Accordingly, back-EMF and phase current multiplication, considering all losses, is the instantaneous power supplied. The motor's input and output power can be expressed as in (12) and (13).

$$P_i = i_a e_b + i_b e_b + i_c e_c \tag{12}$$

$$P_o = P_i - (P_{fw} + P_{cua} + P_t + P_{fe}) \tag{13}$$

where P_i is the input power, P_{fe}, P_t, P_{cua}, and P_{fw} are losses like iron, transistor/diode, stator copper, windage, and frictional losses respectively. The efficiency expression is stated in (14) and is computed by factoring output and input power along with losses.

$$\eta = \frac{P_o}{P_o + P_{fw} + P_{cua} + P_t + P_{fe}} \tag{14}$$

Stray losses are approximately 1% of the Mechanical Power [31] and therefore these have not been considered in calculations.

The torque τ is obtained as shown in (15) is the ratio of power to the angular speed. The torque at any instant of rotor T(θ)is the arithmetic sum of average torque, and torque ripple is represented in (16). The motor's average torque and torque ripple can be stated as in (17) and (18).

$$\tau = P_o/\omega \tag{15}$$

$$T(\theta) = T_{avg} + T_{ripple} \tag{16}$$

$$T_{avg} = \frac{1}{\theta_1' - \theta_1}\int_{\theta_1}^{\theta_1'} T(\theta) \tag{17}$$

$$T_{ripple} = \frac{T_{max} - T_{min}}{T_{avg}} \tag{18}$$

where ω represents mechanical rotation/speed in rad/s, $(\theta_1' - \theta_1)$ represents the complete electrical cycle of the PMBLDC motor. The cogging torque can be minimized by selecting the best value of the rotor pole embrace factor. The pole embrace factor is the ratio of rotor pole pitch (β) pole arc (γ) in a permanent magnet motor, as shown in Fig. 3. Generally, its value is less than unity [32].

4 Design of PMBLDC Motor

A designer can reduce demagnetizing effect and cogging torque with the appropriate selection of permanent magnet materials. Cogging torque generates noise, causes backlash in bearings, and disturbs rotor eccentricity. Table 2 lists the parameters of the permanent magnet materials [33]. Among three materials, the rare earth materials Neodymium Iron and Boron (NdFeB) rare earth magnet material are very high in demand because of greater magnetic field density, better

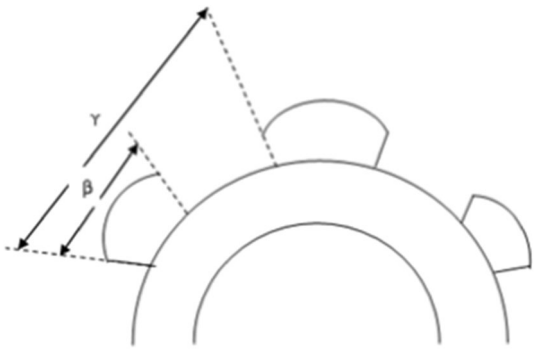

Fig. 3 Rotor pole embrace factor diagram

magnetic field residual density and due to low curie temperature. Samarium Cobalt (SmCo) is the second-strongest magnet material after NdFeB but is the most expensive. Low-cost ceramic magnet materials are easily available and have very low magnetic field density due to poor retentivity. Mostly NdFeB and SmCo are being used for the motors used in EV's. Alnicos have low coercive forces, which get demagnetized easily. Rare-earth permanent magnet materials have opened up new PMBLDC motor design and application options. The selection of magnet materials is purely based on the type of application [33–35]. Airgap length affects the motor performance and hence in addition to mechanical and thermal concerns, choosing the optimum airgap length depends on the objectives of the design and type of applications. In case of EV the increase in air gap length decreases the torque ripple content, while the increased thickness of the magnet helps to avoid demagnetization [21].

The magnitude and frequency of the cogging torque also affect the selection of pole/slot combination. Motors with slot/pole/phase ratio value 1 or higher are integral-slot motors. In fractional-slot motors, as the slot/pole ratio decreases, the magnitude of cogging torque and frequency increases. In other terms, fractional slot motors have reduced cogging torque compared to integral slot motors. As a result, the amplitude of cogging torque reduces and to ensure mechanical utility, a 24/18 (slots/pole) combination is selected for the design having slots/pole/phase ratio less than 0.5 [24].

The design procedure of the BLDC motor is shown in Fig. 4. The outer rotor PMBLDC motor has been designed using ANSYS Maxwell software. Figure 4 depicts the implementation of the adaptive finite element process on the PMBLDC motor. Rmxprt tool of Ansys Maxwell has been used as the designing platform. As per the Indian Driving Cycle (IDC) the motor specifications are selected to propel the cargo weight of EV and overcome the resistive forces. There are three stages of the finite element process in the flow chart. The mesh definition comes under the pre-processing stage of finite element procedure. The motor region under consideration is discretized using different kinds of finite elements, which in our case are the first order triangular elements. Parametric analysis comes under the processing stage of the finite element procedure, whereas different kinds of refinement strategies come under the post-processing stage. Error analysis to get the optimum design of the motor is also a part of the post-processing stage. In this paper h-adaptivity refinement strategy has been used and preferred over the p-type and hp type refinement strategies. The dimensional parameters of the motor once fixed

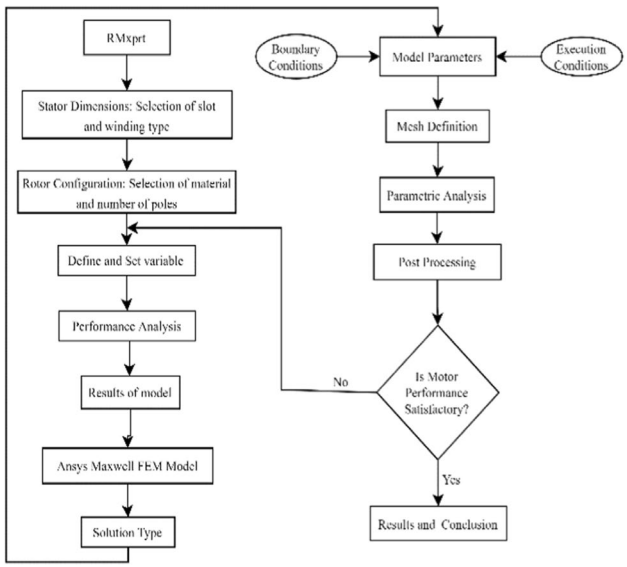

Fig. 4 Flow chart of adaptive finite element process on motor

Table 2 Properties of Permanent magnet material

Properties	Alnicos	Ceramic	Samarium cobalt	Neodymium Iron Boron (NdFeB)
Residual density, B_r (T)	0.7–1.28	0.23–0.41	0.83–1.16	1.00–1.41
Coercive force, H_c (kA/m)	37–143	50–290	480–840	760–1030
Max. energy product, BH_{max} (kJ/m^3)	10.7–71.6	8.35–31.8	130–240	220–366
Density, (g/cm^3)	6.8–7.3	4.9	8.4	7.4
Max. service temp, T_{max} (°C)	450–550	800	300–350	150

Table 3 Dimensional specifications of PMBLDC motor

Parameter	Value
No of pole/slot	24/18
Stator outer diameter (D_{so})	180 mm
Stator inner diameter (D_{si})	90 mm
Stack length (L)	50 mm
Rotor outer diameter (mm)	35.5
Rotor inner diameter (D_{ri})	182 mm
Rated Power	3.5 kW

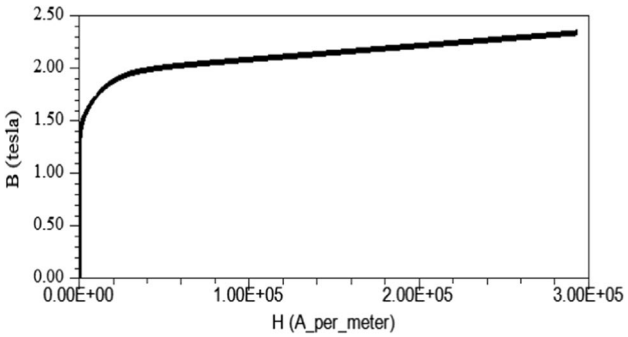

Fig. 5 BH curve of M27_26G silicone steel

are not altered, however the changes as per the feedback received from the post-processing stage are incorporated under "Define and Set variable" block to make the adaptive process. Optimum selection of rotor embrace factor and air-gap length reduces the cogging torque. Dimensional specification of the PMBLDC motor is tabulated in Table 3 [24]. The 24/18 slot/pole combination of this reference paper has been selected over the other slot/pole combinations because less number of slots and poles make motor structure compact and cost-effective. Same slot/pole combination has been considered for the design and analysis of the motor in the present work. For designing a motor, the rotor pole embrace factor is selected as the variable.

The material used for the winding is copper while silicone steel material M27_26G is used for the stator and rotor core. The BH curve of the material is shown in the Fig. 5, B is the magnetic field density in tesla and H is magnetic field intensity in A_per_meter.

5 Parameter Optimization

The cogging torque of the motor must be decreased for a smooth operation. The motor performance can be analyzed from a variety of perspectives. Efficiency is one of the most important characteristics of PMBLDC motor design. This motor is designed for the two-wheeler BEV at a constant

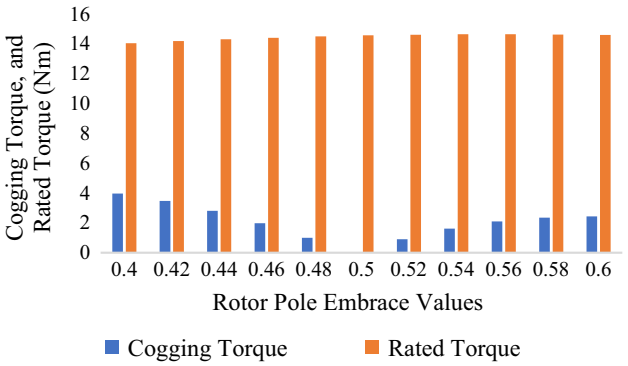

Fig. 6 Graphical representation of cogging torque and rated torque with reference to rotor pole embrace factor

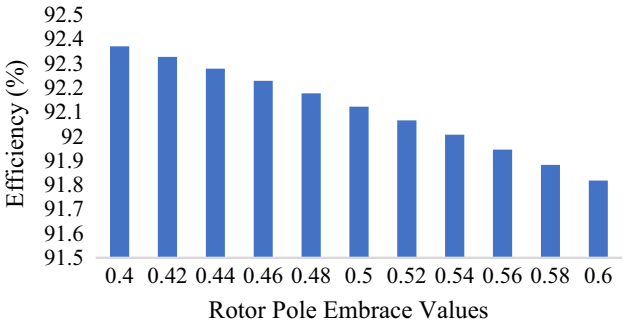

Fig. 7 Graphical representation of efficiency with reference to rotor pole embrace factor

power region of 3.5 kW. The variable rotor pole embrace factor has a considerable influence on the cogging torque and efficiency of the motor. The parametric approach is applied to guide the selection of the pole embrace factor in the design. In the parametric process of optimizing the rotor pole embrace factor values, region of interest must be considered, where efficiency is maximum and cogging torque is minimum. It is not necessary to achieve highest value of efficiency and lowest value of cogging torque at same value of variable. Sometimes the value between different regions needs to be selected. To achieve the optimum values of performance keeping in consideration the size of the motor, the pole embrace factor referred as 'p' is varied from 0.4 to 0.6, considering it as a lower limit and upper limit having 0.02 step size. The cogging torque, rated torque and efficiency with the change in the rotor pole embrace factor value are obtained by parametric scanning as shown in Figs. 6 and 7 respectively. At value 0.5, the cogging torque is least, and its value is 0.0353% of rated torque. Cogging torque is highest at 0.4 and its value is 28.27% of rated torque and at 0.52 its value is 6.1% of rated torque. The graph depicts that cogging torque is lowest at point 0.5 and at the same point efficiency

of the motor is approx. 92.1%. The graphical representation also shows the lowest and intermediate values of the cogging torque and efficiency. The efficiency is highest i.e., 92.37% at pole embrace factor of 0.4 and is lowest i.e., 91.81% at value of 0.6.

The cogging torque variation in respect to the position of rotor is shown in Fig. 8. As shown in the graph the smaller value of cogging torque is 0.005 Nm at point 0.5 and the highest value of cogging torque is 3.967 Nm at point 0.4. The smaller value of cogging torque indicates less speed fluctuations, and better running stability.

The comparison of performance parameters for various values of embrace factor is shown in Table 4. For the propulsion of an electric vehicle at low speed, initially high rated torque is required with enough air gap density. As evident in Table 4 the value of airgap flux density is highest at 0.4 value of embrace factor with less loss. But at some point, the effect of cogging torque is high. Besides, the lowest value occurred at 0.6 embrace factor with maximum losses. With less value of cogging torque and compromising the efficiency of the motor, the optimum intermediate value selected is 0.5 for air gap flux density and average value current. At this value the change in air gap density does not lead to extreme change in winding average current value. Permanent magnet may get demagnetized with abrupt and extreme variations of current and therefore due attention must be given on this parameter. No significant changes in average input current have been noticed while varying the pole embrace factor from 0.4 to 0.6. Most optimum values have been observed at pole embrace factor of 0.5, keeping in view the requirements of battery electric vehicles.

The air gap flux density, average current and rated torque is determined parametrically with change in the embrace factor illustrated in Fig. 9.

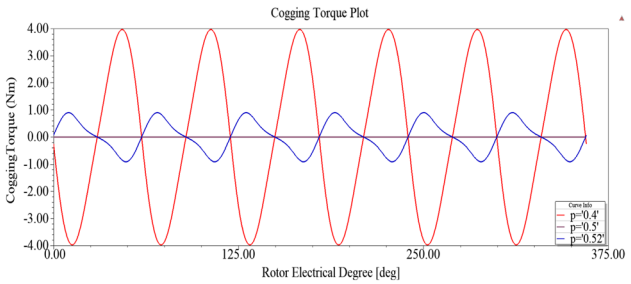

Fig. 8 Variation of cogging torque versus rotor angle in degree

6 Finite Element Based Magnetic Field Analysis of PMBLDC Motor

After electrical analysis, the FEM motor model is created using ANSYS Maxwell using the periodic boundary condition of the motor's inner magnetic field distribution. The FEM model of motor is designed for optimum embrace value of 0.5. A discrete time simulation has been tuned for

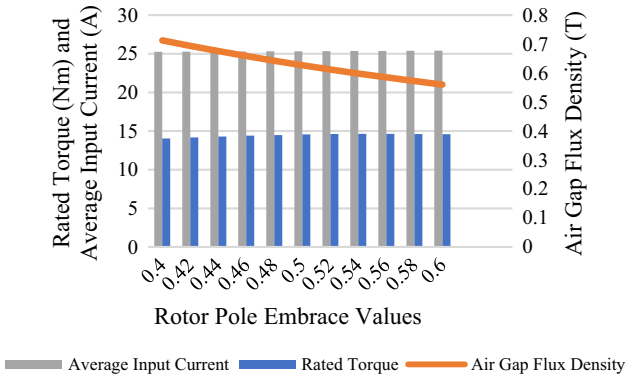

Fig. 9 Graphical representation of air gap flux density, average current and rated torque with rotor pole embrace factor

Table 4 Comparison of performance of the PMBLDC motor at various pole embrace factor

P	Cogging torque (Nm)	Rated torque (Nm)	Efficiency (%)	Airgap flux density (T)	Average input current (A)	Total losses (W)
0.4	3.967	14.03	92.37	0.713	25.26	289.09
0.42	3.470	14.17	92.32	0.694	25.27	290.883
0.44	2.809	14.29	92.27	0.676	25.28	292.849
0.46	1.97	14.40	92.22	0.659	25.30	294.917
0.48	1.003	14.49	92.17	0.642	25.31	297.083
0.5	0.005	14.56	92.12	0.627	25.33	299.332
0.52	0.9009	14.61	92.06	0.612	25.34	301.669
0.54	1.613	14.63	92.00	0.598	25.36	304.104
0.56	2.091	14.63	91.94	0.5853	25.37	306.621
0.58	2.345	14.62	91.88	0.5727	25.39	309.219
0.6	2.432	14.59	91.81	0.5607	25.41	311.896

a time step of 2 ms and a range of 0 to 60 ms. This is subjected to transient analysis at rated load and rated speed. It generates the distribution profile of magnetic field at particular instant of time and rotor position. The structure design of the motor is shown in Fig. 10 and the mesh plot for full fraction model of the design is shown in Fig. 11.

- The distribution of magnetic field density of the motor is shown in Fig. 12 and the magnetic forces acting on the surfaces/edges of the motor is shown in Fig. 13. This elucidates that no saturation occurs in the motor and the maximum density of the magnetic flux exists in the stator tooth tip.

For the optimum design the graph for electromagnetic torque is shown in Fig. 14. The maximum peak value is 57.87 Nm, minimum is 5.06 Nm whereas the average torque value is 50.16 Nm. The value of the ripple torque is 1.25 Nm. The ripple content of the motor at this value is less in comparison to other values which enhance the life span of the motor with less requirement of maintenance. The efficiency of the motor has improved by 1.05%, compared to earlier reported design [24].

The variations in pole embrace factors of rotor led to the variation in unaligned position air gaps and thus providing more flux linkage at aligned position. The phase winding flux linkage and current for rated speed with time is shown in Figs. 15 and 16.

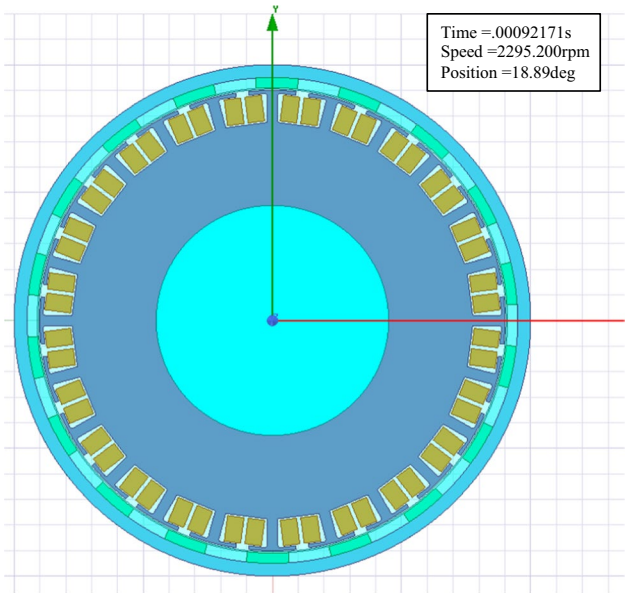

Fig. 10 Structure diagram of the motor

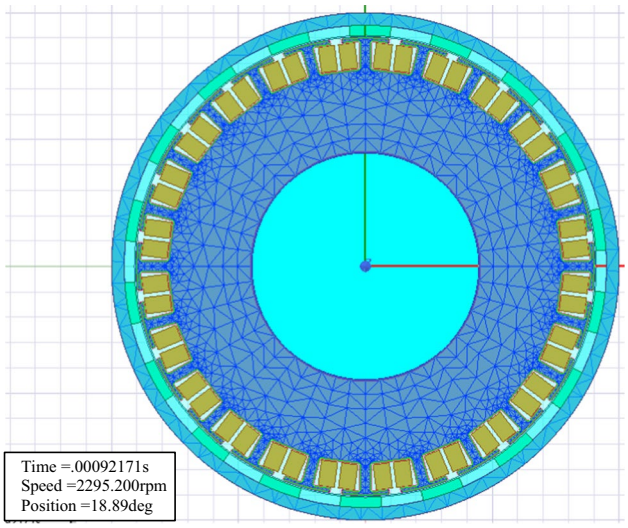

Fig. 11 Mesh refinement of the motor

7 Conclusion

The present work in this paper represents the influence of rotor pole embrace factor on the performance of the motor for battery electric vehicle applications. With the help of a kinematic equation, the parameter matching with the PMBLDC motor has been deduced. Parametric analysis with optimetrics has been applied to accomplish the selection of suitable embrace factors with minimum ripples and maximum efficiency. Finite element based electromagnetic field analysis is performed based on the optimal value of pole embrace factor. The smaller improvement of efficiency has a good impact on the state of health of the battery, which is

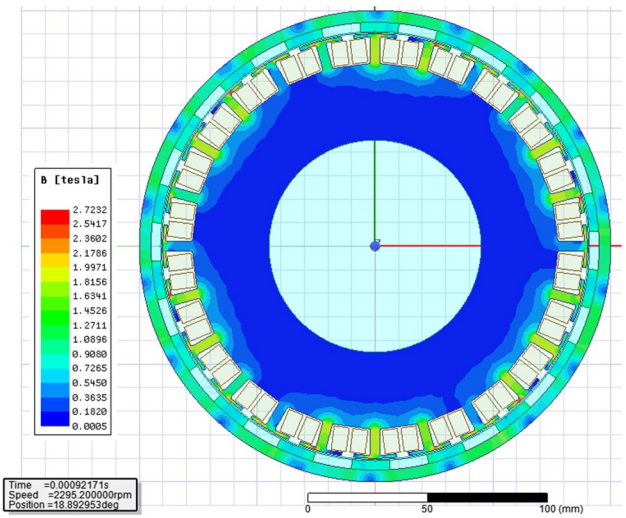

Fig. 12 Magnetic flux density distribution of motor

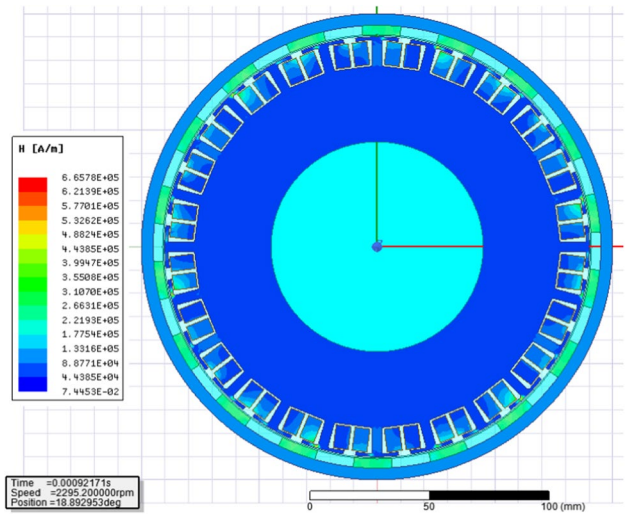

Fig. 13 Vector Potential of the motor

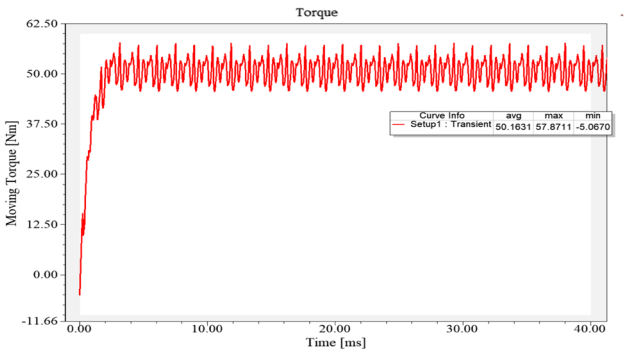

Fig. 14 Plot showing variation torque and time at specific speed

powering the vehicle. The reduction in cogging torque in the proposed design of the motor has a significant role to ensure the smooth drive and overall performance of the electric vehicles. The electromagnetic torque generated by the motor

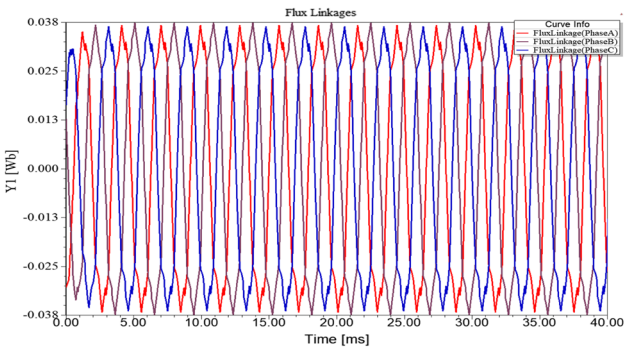

Fig. 15 Winding flux linkage at rated speed

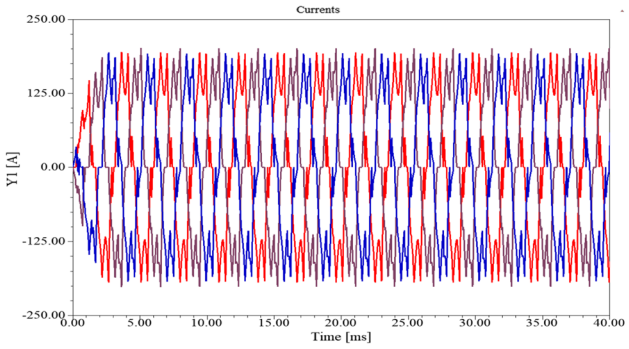

Fig. 16 Winding current for rated speed

is enough to propel the vehicle. Consequently, a reduction in torque ripple reduces acoustic noise and vibrations of the motor and, in turn, lowers the motor's eccentricity disbalancing issue, thereby extending the life span of battery electric vehicles.

Funding Open access funding provided by Eötvös Loránd University.

References

1. Dalal A, Kumar P (2018) Design, prototyping, and testing of a dual-rotor motor for electric vehicle application. IEEE Trans Industr Electron 65(9):7185–7192. https://doi.org/10.1109/TIE.2018.2795586
2. Chen Q, Xiao Q, Liao C, Zeng L, Li X, Huang J, Zhou C (2017) Design and analysis of outer rotor in-wheel motor for micro-electric vehicle. Adv Mech Eng 9(11):1687814017729088. https://doi.org/10.1177/1687814017729088
3. Saidur R (2010) A review on electrical motors energy use and energy savings. Renew Sust Energy Rev 14(3):877–898. https://doi.org/10.1016/j.rser.2009.10.018
4. Sandeep V, Shastri S (2019) Analysis and design of PMBLDC motor for three wheeler electric vehicle application. In: E3S web of conferences, 87, 1022. EDP Sciences. https://doi.org/10.1051/e3sconf/20198701022

5. Singh B, Singh S (2009) State of the art on permanent magnet brushless DC motor drives. J Power Electron 9(1):1–17
6. Jiang C, Qiao M, Zhu P, Zheng Q (2018) Design and verification of high speed permanent magnet synchronous motor for electric car. In: 2018 2nd IEEE Advanced Information Management, Communicates, Electronic and Automation Control Conference, (pp. 2371–2375). IEEE. https://doi.org/10.1109/IMCEC.2018.8469398
7. Jang SM, Jeong SS, Ryu DW, Choi SK (2001) Design and analysis of high speed slotless PM machine with Halbach array. IEEE Trans Magn 37(4):2827–2830. https://doi.org/10.1109/20.951319
8. Singh B, Singh BP, Dwivedi S (2006) A state of art on different configurations of permanent magnet brushless machines. J Inst Eng India Part E Electr Eng Div 87:63
9. Jokinen T, Hrabovcova V, Pyrhonen J (2013) Design of rotating electrical machines. Wiley, Amsterdam
10. Sumithra P, Thiripurasundari D (2017) Review on computational electromagnetics. Adv Electromagn 6(1):42–55
11. Kumar A, Marwaha S, Singh A, Marwaha A (2009) Performance investigation of a permanent magnet generator. Simul Model Pract Theor 17(10):1548–1554. https://doi.org/10.1016/j.simpat.2009.05.005
12. Kumar A, Marwaha S, Singh A, Marwaha A (2010) Comparative leakage field analysis of electromagnetic devices using finite element and fuzzy methods. Expert Syst Appl 37(5):3827–3834. https://doi.org/10.1016/j.eswa.2009.11.036
13. Kumar A, Marwaha S, Marwaha A, Marwaha A (2009) Comparative mechanical dynamic analysis of permanent magnet generator using finite element and fuzzy methods. Open Autom Control Syst J. https://doi.org/10.2174/1874444300902010008
14. Kumar A, Marwaha S, Marwaha A (2006) Comparison of methods of minimization of cogging torque in wind generators using FE analysis. J Indian Inst Sci 86(4):355
15. Sadiku MN (2000) Numerical techniques in electromagnetics. CRC Press, Boca Raton
16. Zienkiewicz OC, Taylor RL, Zhu JZ (2005) The finite element method: its basis and fundamentals. Elsevier, Newyork
17. Chan CC, Chau KT (1991) Design of electrical machines by the finite element method using distributed computing. Comput Ind 17(4):367–374. https://doi.org/10.1016/0166-3615(91)90049-F
18. Guo L, Wang H (2021) Research on stator slot and rotor pole combination and pole arc coefficient in a surface-mounted permanent magnet machine by the finite element method. World Electr Veh J 12(1):26. https://doi.org/10.3390/wevj12010026
19. Li Y, Qu B, Zhu Y, Wan Y, Zhu X (2019) Design and analysis of an outer rotor flux switching permanent magnet machine for light electric vehicles. Int J Appl Electromagn Mech 62(1):161–172. https://doi.org/10.3233/JAE-190079
20. Yuan Y, Meng W, Sun X, Zhang L (2019) Design optimization and analysis of an outer-rotor direct-drive permanent-magnet motor for medium-speed electric vehicle. World Electr Veh J 10(2):16. https://doi.org/10.3390/wevj10020016
21. He C, Wu T (2019) Analysis and design of surface permanent magnet synchronous motor and generator. Ces Trans Electr Mach Syst 3(1):94–100. https://doi.org/10.30941/CESTEMS.2019.00013
22. Popescu M, Goss J, Staton DA, Hawkins D, Chong YC, Boglietti A (2018) Electrical vehicles—practical solutions for power traction motor systems. IEEE Trans Ind Appl 54(3):2751–2762. https://doi.org/10.1109/TIA.2018.2792459
23. Patel AN, Suthar BN (2018) Design optimization of axial flux surface mounted permanent magnet brushless dc motor for electrical vehicle based on genetic algorithm. Int J Eng 31(7):1050–1056
24. Cabuk AS, Sağlam Ş, Üstün Ö (2017) Impact of various slot-pole combinations on an in-wheel BLDC motor performance. IU J Electr Electron Eng 17(2):3369–3375
25. Li Y, Lu Q, Zhu ZQ, Wu D, Li G (2016) Superposition method for cogging torque prediction in permanent magnet machines with rotor eccentricity. IEEE Trans Magn 52(6):1–10. https://doi.org/10.1109/TMAG.2016.2533361
26. Nanekaran RN (2014) Shape optimization of the permanent magnet pole of the brushless dc motor by fem. Electr Power Eng Front 3(3):16–24
27. Larminie J, Lowry J (2012) Electric vehicle technology explained. Wiley, Hoboken
28. Ehsani M, Gao Y, Longo S, Ebrahimi KM (2018) Modern electric, hybrid electric, and fuel cell vehicles. CRC Press, Boca Raton
29. Hanselman DC (2003) Brushless permanent magnet motor design. The Writers' Collective, Cranston
30. Yildirim M, Kurum H, Miljavec D, Corovic S (2018) Influence of material and geometrical properties of permanent magnets on cogging torque of BLDC. Eng Technol Appl Sci Res 8(2):2656–2662. https://doi.org/10.48084/etasr.1725
31. Utomo SB, Irawan JF, Hadi W, Sastiko BA (2021) Design of 6S8P axial flux permanent magnet brushless DC motor with double-sided rotor. In: IOP Conference Series: Materials Science and Engineering, 1034(1), 012053
32. Marwaha S, Rupam (2021) Mitigation of Cogging Torque for the Optimal Design of BLDC Motor. In: 2021 IEEE 2nd International Conference On Electrical Power and Energy Systems (ICEPES) (pp. 1–5). IEEE. https://doi.org/10.1109/ICEPES52894.2021.9699544
33. Miller TJ (1989) Brushless permanent-magnet and reluctance motor drives. Oxford University Press, Oxford
34. Trout SR (2001) Material selection of permanent magnets, considering thermal properties correctly. In: Proceedings: Electrical Insulation Conference and Electrical Manufacturing and Coil Winding Conference (Cat. No. 01CH37264) (pp. 365–370). IEEE. https://doi.org/10.1109/EEIC.2001.965683
35. Ruoho S, Kolehmainen J, Ikaheimo J, Arkkio A (2009) Interdependence of demagnetization, loading, and temperature rise in a permanent-magnet synchronous motor. IEEE Trans Magn 46(3):949–953. https://doi.org/10.1109/TMAG.2009.2033592

Rupam Bansal received her B.Tech degree in Electrical Engineering in 2014 from Punjab Technical University, Jalandhar, India and M.Tech degree in Power Engineering in 2016 from Guru Nanak Dev Engineering College, Ludhiana, India. Currently, she is pursuing Ph.D. degree in Electrical and Instrumentation Engineering Department, SLIET, Longowal, Punjab, India. Her current research area

of interest is Machine Design, Electric Vehicles Application, and Renewable Sources.

Dr. Sanjay Marwaha received the Bachelor of Engineering (Electrical) degree from Gorakhpur University, Gorakhpur, India, in 1988, the Master of Engineering (Power System) from Punjab University, Chandigarh, India, in 1990, and the Ph.D. degree from Guru Nanak Dev University, Amritsar, India, in 2000. He is working as professor in the Department of Electrical and Instrumentation Engineering at Sant Longowal Institute of Engineering and Technology, Longowal, India since year 2002. His areas of interest include Design and Analysis of Electromagnetic Devices, Electrical and Electronic Measurement and Instrumentations, Electrical Machines, Power Systems, and High Voltage Engineering. He is having 175 research papers in his credit, which have been published in International and National journal as well as International and National conference proceedings of repute.

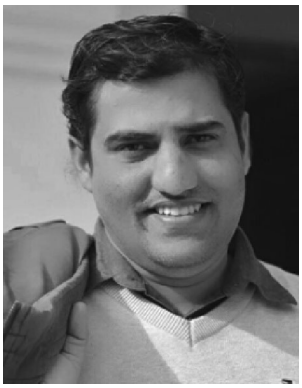

Chaman Verma is working as an Assistant Professor and the Ph.D. Candidate with the Department of Media and Educational Informatics, Faculty of Informatics, Eötvös Loránd University, Hungary. He has been awarded a Research Scholarship "ÚNKP, Ministry of Innovation and Technology (MIT), and National Research, Development and Innovation (NRDI) Fund, Hungarian Government," for the years 2021-2022, and 2022-2023. From 2018 to April 2022, he worked as a Professional Assistant in the EFOP Project, which was co-funded by the European Union and the Hungarian Government. His current research interests include optimization and feature engineering, statistical analysis, machine learning, real-time systems, deep learning, computer vision, health care, educational informatics, and sickness prediction. He is a guest editor of reputed journals. He is also an editorial board member and a reviewer of several scientific conferences and international publications. He has Scopus citations 495 with H-index 14. He has Web of Science citations 78 with H-index 8.